Design of a Green Sunshade: An Entrepreneurial Approach

Danish Rehman
Department of Energy Engineering and Management,
Instituto Superior Tecnico (IST), Lisboa, Portugal
danish.rehman@tecnico.ulisboa.pt

Abstract*—The objective of current work is to design a wind resistant solar sunshade as a part of product development cycle. Importance of simulating the neutral atmospheric boundary layer in CFD for accurate estimation of wind forces over low rise structures has been explained. For validation of boundary conditions we perform flow analysis past a low rise Texas Technical University (TTU) building and compare our results to that of field, experimental and other numerical studies. It is shown that chosen set of boundary conditions result in a reasonably good approximation of pressure field around the building. Using the same set of boundary conditions we simulate flow past sunshade at a $Re = 3 \times 10^6$ with 14.5% turbulence at the height of sunshade. 9 different wind incidence angles are simulated from 0^o to 240^o with 30^o interval to find out the extreme loading scenario. Results show that extreme loading is experienced at angles of 30^o and 0^o whereas all other loading profiles are encompassed in these two. Therefore we perform full scale CFD analysis at 0^o and 30^o so that generated pressure field can readily be used for defining structural loads. Area weighted average of pressure at 5 sub-regions of sunshade are calculated and are used for verifying structural integrity. We then perform FE analysis on two design schemes using reinforced plain weave glass fabric composite and industrial aluminum. Results have shown that composite is not suitable for the current application. Metallic design promises a lightweight and cheap solution for the sunshade under study and will be followed for manufacturing.

I. Introduction and Literature Review

Current work is being carried out as a part of product development for a small startup struggle. The company follows the ideology of integrating sun power in daily commodities which will serve the long time purpose of changing attitudes of people. The Goal is to offer green solutions serving aesthetic need of customers along with clean energy. To enter the market, we decided to offer a solar integrated sunshade (parasol), a shadow space addressing beaches, hotels and individual opinion leaders as target groups. Main achievements while writing business plan were to define a niche market for the proposed solution and validation of business model through detailed interviews conducted at Mykonos Island, Greece from luxury hotels owners. During conducted interviews, a commonly shared concern was related to the strength of the conventional umbrellas. This has lead us to investigate the wind forces on designed sunshade that can be ultimately used for structural integrity verification. Designed sunshade can be seen in Fig.1 where a small solar module is attached on top to provide ample energy for charging hand held devices.

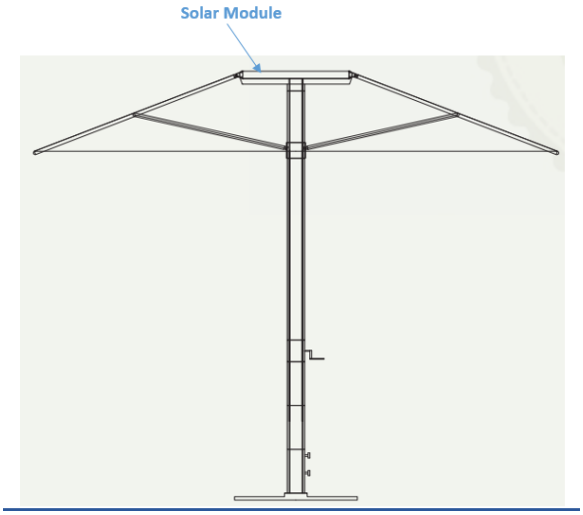

Figure 1: An example of solar integrated sunshade design.

To estimate the wind forces correctly it is necessary to review numerical studies for flow physics of the lower portion of the atmosphere where all the low rise structures interact with wind. Computational studies to understand the effect of turbulent Atmospheric Boundary Layer (ABL) are multidisciplinary ranging from pollutant dispersion modeling to pressure loadings on low rise structures. Mathews [1] predicted the wind generated pressure distribution around a building for natural ventilation studies and concluded that extension of his work can simulate flow around complex buildings. While commenting on his work, Richards and Younis [2] pointed out inconsistencies in turbulence model and

inflow boundary condition equations. They argued that defining inflow velocity profile using empirical power law is not coherent with turbulent model and this results in degradation of flow throughout the domain. Due to this degradation actual intended flow properties do not reach near the point of interest in computational domain that raises a question on the results. Later Richards and Hoxey [3] presented consistent set of boundary conditions for fully developed neutral ABL where horizontal velocity profile is given by log law instead of empirical power law. Their inflow profiles of velocity, turbulent kinetic energy and eddy dissipation rate were consistent with standard $k-\epsilon$ model and showed no degradation of flow in computational domain. Since then these set of inflow conditions have been used by numerous researchers [4] investigating flows inside neutral ABL using RANS turbulence models. However researchers have reported various difficulties while implementing profiles suggested by [3]. Zhang [5] reported an unwanted change in mean wind profile and especially turbulent kinetic energy using standard $k-\epsilon$ model and standard wall functions to resolve the boundary layer near the ground. While simulating flow on a backward facing step, he argued that such numerical errors can give rise to serious errors in the pressure and velocity estimations. As modeling of neutral ABL is vital to various engineering fields therefore a required guide to implement boundary conditions proposed by Richards and Hoxey [3] in CFX and Fluent was first presented by Blocken [6]. A common practice to report the field surface roughness for ABL is to specify aerodynamic roughness length as done by [7] whereas CFX and Fluent define rough wall (required for ground boundary) using an equivalent sand grain roughness. This sand grain roughness is further utilized by wall functions for resolving boundary layer near the ground by software. Blocken presented relationship between aerodynamic roughness and sand grain roughness for Fluent and CFX both which helped him to get a stratified neutral ABL. Richards and Hoxey [8] revisited their consistent inflow conditions for $k-\epsilon$ model considering numerous difficulties for application to commercial codes by various authors. They presented implementation of homogeneous ABL in CFX with a number of eddy viscosity models along with a Reynolds stress model (QI) and showed that to avoid over estimations in computational engineering problems, Reynolds stress models should be further explored in case of RANS modeling.

Computational wind engineering models have also been used to study forces on structures other than buildings placed within the ABL. A detailed review for the application of CFD in computational wind engineering has been provided by Aly [4]. In his earlier study [9], author performed wind tunnel and computational modeling to find pressure loadings on ground mounted solar panels placed in ABL. Scaled wind tunnel experiments and CFD to mimic these test conditions were performed using LES. He concludes that mean pressure coefficients on low rise structures do not change with model scale and neither with turbulence content in the incoming flow. Wind flow characteristics for a solar panel attached on roof top of a low rise building is studied by Pratt and Kopp [10] using atmospheric boundary layer wind tunnel. They concluded that interaction of ABL with small architectural features should be considered as in case of studies where roof mounted PV arrays are not modeled above buildings will not yield correct peak uplifts. Shademan and Hangan [11] conducted a numerical study to estimate the wind force coefficients on stand alone and arrayed ground mounted solar panels. They used empirical power law with maximum speed as provided in ASCE07 [12] with turbulence intensity of 16% at the inlet and provided values of force coefficients that can be used in design of such configurations. Later a wind tunnel and computational study is carried out on a single and array mounted configurations of solar panels by Bitsuamlak et.al [13]. They used LES for turbulence modeling and found out that CFD underpredicted the wind loads in general in four different cases of angle of attack variation. Gumley [14] conducted a parametric wind tunnel study to understand the effect of various parameters on mean and peak pressure loadings over free standing canopies. He performed all his experiments with a velocity profile of rural terrain ($z_o = 30mm$). Results showed that UK code for wind loading used at that time underestimated wind loading for such structures and therefore may lead to design failures. In a recent experimental and numerical study conducted by Poitevin et. al [15], authors demonstrated the incapability of ASCE07 code [12]for estimation of wind loading on open canopy structures with parapets and stated that ASCE07 recommendations are not sufficient to carry out the safe design of such structures.

Pressure field loading on a metallic roof of $6m$ height is conducted by Diaz. et al. [16, 17] where authors utilize finite element and finite volume methods to estimate the wind loads. A detailed literature review to estimate wind loadings on an agricultural net is conducted by Briassoulis et. al [18]. They propose a methodology to integrate these wind loadings in structural analysis to achieve low cost optimised structures. Nets are modeled as orthotropic membranes and analyzed using FEM.

Uniform pressure loads were applied on the orthotropic nets and results on the accompanied structure were detailed. Authors conclude that design criteria requires a change in EU standard for green house system to include net supporting structures. To gauge the effectiveness of current static structural analysis practices in industry against wind loading, Schell et. al. [19] performs non linear wind response history analysis over solar arrays. Experimentally observed dynamic wind data was used to analyze the transient structural response of solar array and it has been concluded that current codes of static structural analysis are appropriate design tools defining wind loads and required strength of structural members. A thin membrane structure of $29m$ span umbrella has been analyzed using coupled fluid structure interaction by Michalski et. al [20, 21]. Mean wind flow characteristics were observed in a full scale experimental facility in Germany for one complete year. LES was then utilized to model neutral atmospheric boundary layer representing observed velocity and turbulence at the height of umbrella. Computational structural dynamics results showed a variation of $\pm 25\%$ in deflections observed at experimental facility. It was an industrial project performed to set standards for computational coupled models for thin structures design. The Computational model overall showed a reliable agreement with experimental study.

Numerical methodology for CFD and FEA is explained in the next section. A validation study is performed for estimating pressure loading over a low rise structure in section 3. Computational results for sunshade being investigated are presented along with the discussion in section 4. Section 5 presents conclusions drawn out of current work along with future work recommendations.

II. Numerical Methodology

A. Flow Analysis

The flow in the current problem is governed by the incompressible continuity and momentum (Navier-Stokes) equations, which can be represented as follows:

Continuity Equation

$$\frac{\partial u_i}{\partial x_i} = 0 \tag{1}$$

Momentum Equation

$$\frac{\partial u_i}{\partial t} + \frac{\partial}{\partial x_j}(u_j u_i) = -\frac{1}{\rho}\frac{\partial p}{\partial x_i} + \nu \frac{\partial^2 u_i}{\partial x_j \partial x_j}, \tag{2}$$

where i,j=1,2,3; the u_i represents the Cartesian velocity components (u,v,w) in longitudinal, lateral and normal directions; p is the pressure; ρ is the fluid density; and ν is the fluid kinematic viscosity. As there is no on site mean wind speed measurements available, we use a mean wind speed of $20\frac{m}{s}$ at the height of the sunshade $H = 2.5m$ above the ground. The selected mean wind speed corresponds to *strong gale* and on a modern Beaufort scale, it represents wind scale of 9. Such a high speed is selected in order to estimate the wind loads that will be representative of storm loading in real scenario. Thus based on the chord length (L), Reynolds number ($Re_L = \frac{U_{ref}L}{\nu}$) of 3×10^6 is simulated. Governing equations are non dimensionalized using mean wind velocity (U_{ref}) as velocity scale and chord length of sunshade (L) as length scale. Turbulence intensity and representative terrain roughness is also assumed to be the same as of validation study measured in field data [22] of TTU building. These conditions generate slightly less than 16% turbulent intensity at the height of the sunshade which is commonly reported turbulence level in open terrain studies using an empirical power law as used in [11, 13].

For current CFD study only top cap is used without any attachments underneath. Modeled sunshade is placed in a computational domain of ($20L \times 10L \times 6L$) where $L = 2.5m$ is the chord length of the sunshade. Domain size and associated boundary condition modeling is shown in Fig. 2(a). Guidelines provided by (AIJ) [23] and COST [24, 25] and COST are considered for domain size selection. Domain and sunshade are meshed using a similar strategy as before to have more cells near the point of interest (sunshade) and coarse towards far field. The discretized computational domain is shown Fig. 2 where an unstructured mesh using tetrahedral elements is used in the vicinity of sunshade with dense mesh near the edges and relatively coarse over the roof surface as shown in Fig.2(c). Number of elements are systematically increased in mesh convergence study using the similar mesh strategy to check the results dependency on mesh.

Steady state RANS simulations were used in neutral ABL verification and mesh convergence studies. For turbulence model comparison in validation study, unsteady RANS simulations are employed. For discretization of convection term in Navier Stokes equation we use high turbulence scheme available in ANSYS CFX whereas second order backward Euler scheme is used for temporal discretization. Simulation is run for a non dimensional time ($t^* = \frac{tU_{ref}}{H}$) of 15 with non dimensional time step of 0.025. Such timestep is sufficient to resolve necessary flow details. Convergence criteria for each outer loop iteration is set as 1×10^{-4} for all residuals. Results are averaged after initial 20 timesteps. These

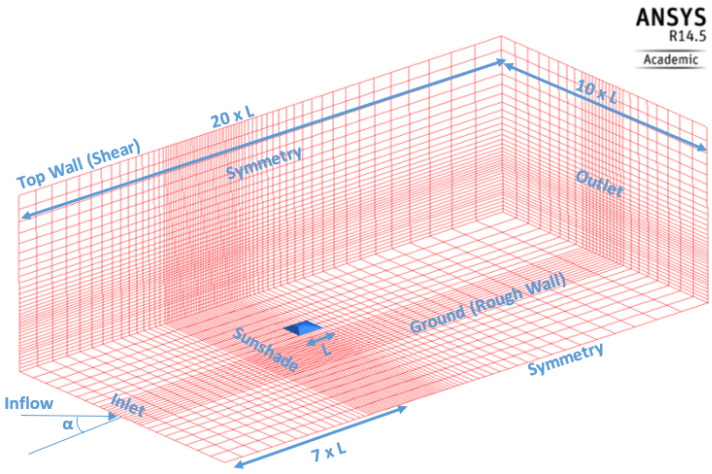

(a) Domain size and boundary conditions

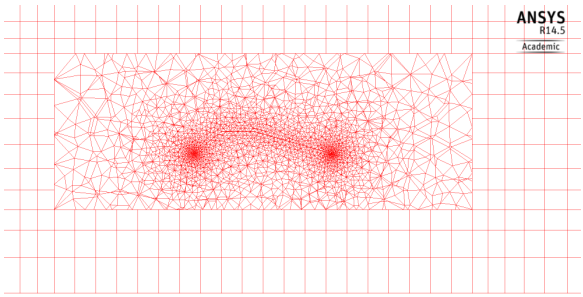

(b) Zoomed view for mesh around sunshade on the center plane of domain

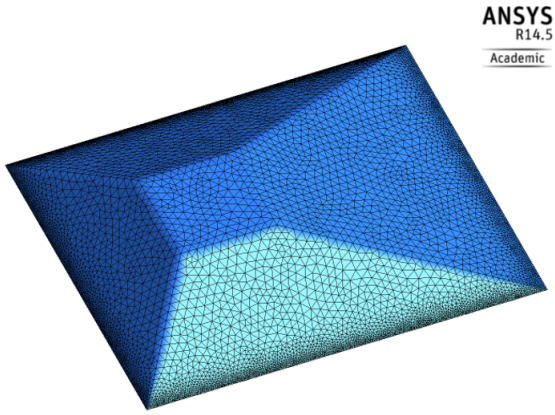

(c) Sunshade surface mesh

Figure 2: Computational mesh details of CFD model

settings for unsteady RANS are kept same in current work unless otherwise mentioned.

B. Structural Analysis

FEA is utilized to investigate response of sunshade structure under wind loads. Two alternative design schemes are explored using static structural analysis. In first scheme we use fiber reinforced composite with plain weave E glass fabric for the top cap of umbrella and second strategy involves conventional Aluminum design. All the modeling and analysis is performed in ANSYS Mechanical APDL software. Top cap of sunshade is modeled using shell element (Shell181) which is a four node element with six degrees of freedom at each node that is three translational motions and three rotational around x, y and z axes [26]. It can support a lay up scheme required to model composites. We also employ Beam element (Beam188) to model the metallic cross section to be used in the design of top cap of sunshade for case of Aluminum design. Beam188 also has six degrees of freedom at each node and can be assigned any cross sectional area from solid square to a pipe of certain thickness. To capture the non linearity in numerical setup, large deformation is turned on in ANSYS as followed by [17, 19, 27]. Application of the load is divided in ten sub steps and maximum of 500 steps are allowed for numerical convergence. In case solution is not converged during these iterations, it stops and problem is investigated for failure.

In the current study we use plain weave fiber glass fabric reinforced with vinyl ester resin. Material properties for the composites are strongly dependent on the fiber to

resin ratio and varies from one sample to another. In case of orthotropic materials like composite, 9 engineering constants are used to define material completely which are presented in TableI derived from [28]. The ultimate strength of the material in tensile (σ_t) and compressive (σ_c) direction is 280MPa and 180MPa respectively [29]. Similar properties are also mentioned in [30]. Density (ρ_{comp}) of the cured composite part is taken as $1.6\frac{g}{cm^3}$.

Conventional design of sunshade employs metallic structure and is therefore explored to compare the outcome of composite studies. Aluminum metal due to its high strength and recycle-ability at the end of life cycle is considered in current application. The aluminum frame is modeled using beam elements as explained earlier in ANSYS and shown in Fig.3. A cross section of hollow square aluminum pipes is used from the catalogue of supplier (Alumil Aluminum [31]) with various dimensions of thickness until a reasonable solution is achieved. A log file is maintained which allows to change dimensions of selected profile and other solution procedures for iterative study. Material properties and final cross section chosen for the study are summarized in TableII and TableIII.

To distribute the applied pressure load on the load carrying beam members, a thin metallic skin of $1mm$ thickness is modeled and is coupled with the nodes of load carrying members so that there is no independent movement between beams and top skin. Applied boundary conditions are shown in Fig.4 where pressure loading is not shown, however it is applied normal to the surfaces of sunshade according to methodology explained in next sections.

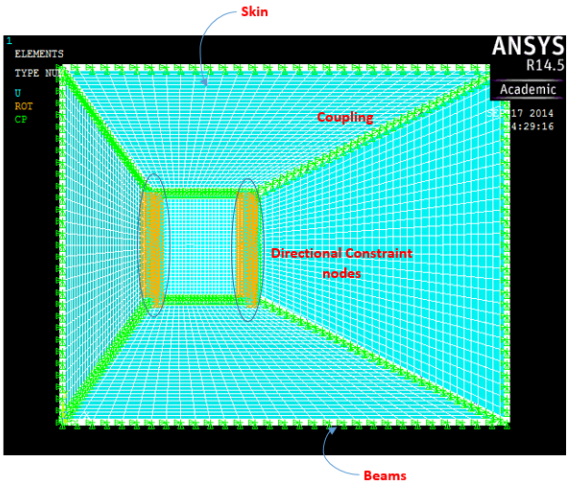

Figure 4: Deformation and coupling constraints applied to the FE model

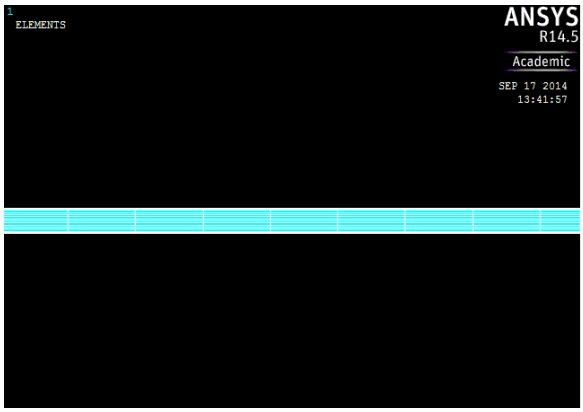

(a) Load carrying member with beam element

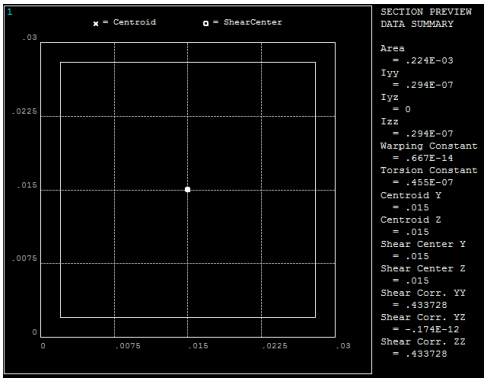

(b) Modeled cross section in ANYS

Figure 3: Modeling of structural members in ASNYS using beam element

Table II: Material properties of Aluminum

E (GPa)	ϑ
73	0.33

III. Validation Study

In a CFD study, computational results are often compared with on site data measurement which is not the case always, therefore wind tunnel simulations are carried out on scaled models to validate the computational estimations. In a design case where neither full scale nor model scale data is available, high quality data sets already published in the literature should be used for validation studies [32]. Therefore in this section we validate numerical model settings and boundary conditions essential to simulate neutral ABL correctly and estimation of wind mean pressure over a low rise building which in our case is TTU buidling immersed in a turbulent neutral ABL is presented. To estimate the pressure loadings as a

Table I: Material properties of used composite [28]

E_x (GPa)	E_y (GPa)	E_z (GPa)	G_{xy} (GPa)	G_{yz} (GPa)	G_{zx} (GPa)	ϑ_{xy}	ϑ_{yz}	ϑ_{zx}
26.66	21.07	10.75	5.17	5.05	5.04	0.13	0.34	0.13

Table III: Cross sectional details of load carrying members

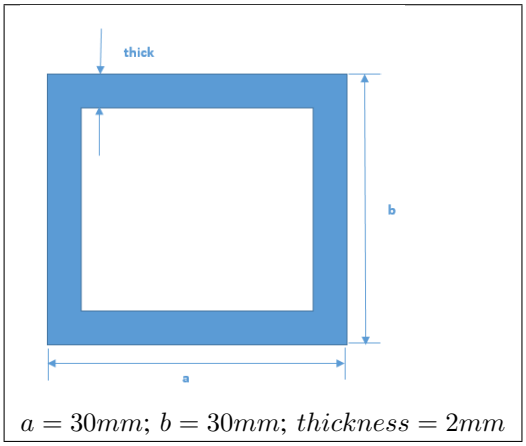

$a = 30mm$; $b = 30mm$; $thickness = 2mm$

result of wind interaction, several wind tunnel facilities were developed e.g. [33, 34]. One such experimental facility is TTU building located at Wind Engineering Research Field Laboratory (WERFL) in the high planes of Lubbock, Texas, USA [35]. Building has dimensions (L x B x H) of $9.1m \times 13.7m \times 4.0m$ with almost straight roof top. Building can be rotated allowing for various wind angle of attacks for pressure investigations [36]. Flow is essentially governed by eqs. 1-2. We employ a structured mesh locally refined near building surfaces. Number of elements are varied in mesh convergence study, however strategy is kept same as shown in Fig. 5. Unsteady and steady RANS simulations are performed according to settings described in previous section.

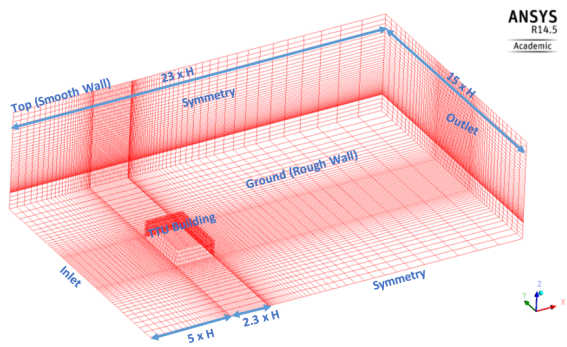

Figure 5: Computational domain and mesh strategy for TTU building

The computational domain is modeled according to recommendations by Architechtural Institute of Japan (AIJ) [23] and COST [24, 25], as $23H \times 15H \times 6H$ where $H = 4m$ is the height of the building. To minimize the streamwise gradients or horizontal homogeneity problem, building upstream length should be as minimum as possible (ref). Ref. [35] uses upstream length of $3.85H$ whereas we employ upstream length of $5H$ for proper development of boundary layer. Lateral and top boundaries as suggested by [23] should be atleast 5H away from the target building in each dimension. We use $5.8H$ for lateral boundary on each side of target building and $6H$ for the top boundary. In the current work 90° angle of attack is simulated which corresponds to the flow parallel to the short wall ($9.1m$) of TTU building [22, 37]. Therefore normalized dimensions of TTU building modeled are $2.3H \times 3.4H \times H$ within the flow domain. Downstream length behind the building should be at least $10H$ [23, 24] whereas we use length of $15.7H$. Boundary conditions applied to the computational model are as follows:

- *Inlet*: The mean free stream velocity (U_{ref}) recorded in field measurements by [7] is $8-10\frac{m}{s}$ and turbulence intensity is $16-20\%$ at the building height of $4m$ that translates in Reynolds number (Re) of 2.5×10^6. We simulate $Re = 3 \times 10^6$ based on the dimensionless velocity $\frac{U}{U_{ref}}$ at dimensionless height H of the building. As discussed before RANS closure modeling is used in the current study and consistent inlet profiles for $k-\epsilon$ model presented by [3] and revisited in [8] given by eqs. 3-6 are used at the inlet boundary condition.

  Horizontal Velocity Equation

$$\bar{u}(z) = \frac{u_*}{\kappa} \ln\left(\frac{z}{z_o} + 1\right) \tag{3}$$

  Turbulent Kinetic Energy Equation

$$K(z) = \frac{{u_*}^2}{\sqrt{C_\mu}} \tag{4}$$

  Eddy Viscocity Dissipation Equation

$$\epsilon(z) = \frac{{u_*}^3}{\kappa(z + z_o)} \tag{5}$$

Frictional Velocity Equation

$$u_* = \frac{\kappa \bar{U_H}}{\ln\left(\frac{H}{z_o} + 1\right)} \tag{6}$$

where K(z) and $\epsilon(z)$ are turbulent kinetic energy and eddy viscosity profiles and C_μ is a model constant having a value of 0.09 taken from [3]. Values of κ can be found for each variation of eddy viscosity models in [8] which in general stays between 0.41 to 0.433. $\bar{U_H}$ is the horizontal mean velocity at height of the object H (z=H).

- *Ground Boundary*: Representation of building surroundings should be modeled either by using small obstacles upstream of target building or specifying appropriate aerodynamic roughness (z_o) for the ground boundary [23]. Dimensionless aerodynamic roughness for our work is calculated by matching Jenson number ($J = \frac{H}{z_o}$) of 240 from wind tunnel tests [34, 35] to be 4.17×10^{-3}. Alternatively [7] also provides roughness length to be $17mm$ which upon non dimensionalizing by height ($H = 4m$) comes out to be the same. However to model the roughness, wall function approach in CFX which is an extension of the method developed by [38] requires equivalent sand grain roughness (K_s) to be specified instead of z_o [26]. Therefore it is necessary to define a relation between K_s and z_o which according to [39] should be $K_s >= 12.5 z_o$. Ref. [40] uses $K_s = 20 z_o$ in their work, therefore it varies from code to code. For ANSYS CFX, this can be achieved by first order matching of ABL mean velocity profile with the wall function velocity profile at point 'P' adjacent to the ground wall and is given by $K_s = 29.6 z_o$ [6]. Thus no slip boundary condition with dimesionless $K_s = 0.1234$ is set at ground for achieving horizontal homogeneous neutral ABL profiles.
- *TTU Building*: No slip wall boundary condition is given for TTU building which essentially makes flow particles stationary at the surface of building.
- *Outlet*: Relative pressure of 0Pa is applied at the outlet boundary condition for the smooth exit of flow out of domain. This employs that gradients of all flow variables at the exit are 0. Please note that reference pressure of $1atm$ is set for all CFX simulations.
- *Side Walls and Top Wall*: A symmetry boundary condition is employed at the side walls which does not allow flow to exit the domain by setting normal components of the velocity as zero. If the computational domain is large enough then lateral and top wall boundary conditions do not affect the results around the buildings [41, 42], whereas free slip wall (inviscid wall condition) with large computational domain will make computation more stable [23]. Thus top wall is modeled as free slip wall with a constant shear stress of $\rho {u_*}^2$ for homogenous ABL as recommended by [3, 8, 39, 40, 43] where u_* is characteristic velocity given by eq. 6. For consistency values of turbulent kinetic energy ($K(z)$) and eddy dissipation rate ($\epsilon(z)$) should be fixed or provided [6]. This can be done by specifying sources of kinetic energy and dissipation in the form of fluxes through top boundary using eq. 7 [8].

$$\frac{\mu_T}{\sigma_e}\frac{d\epsilon}{dz} = -\frac{\rho {u_*}^4}{\sigma_e z} \tag{7}$$

where σ_e is a model constant with value of 1.1 for standard $k-\epsilon$ model and μ_T is modeled turbulent viscosity calculated at the top of the domain using following relation. Vertical flux for turbulent kinetic energy is set as zero. For analytical understanding of these boundary conditions and model constants, please refer to [8].

$$\mu_T = \frac{\rho {u_*}^4}{\epsilon(z)} \tag{8}$$

A. Neutral ABL

As already discussed, ensuring horizontal homogeneity of inflow velocity and turbulence profiles is vital for computational wind engineering [6, 39]. Therefore the boundary conditions discussed before are applied without TTU building inside the domain. The domain is meshed in same strategy as shown in Fig.5. A structural mesh of $74 \times 52 \times 34$ is employed which gives 123760 hexahedral elements and 144540 nodes. For advection term and temporal discritization, default high resolution scheme available in ANSYS CFX is used. A steady state solution using $k-\epsilon$ turbulence model is run. Convergence criteria for all the residuals is set to be 1×10^{-6}. After reaching convergence, simulation was continued for more iterations till the time there is no significant change in residuals further. Furthermore during the mesh it is considered to place the first cell 'P' above the ground boundary such that $z_P > K_s$ as physically it does not make sense to put the first cell into the wall boundary layer [6, 26]. Turbulent intensity is calculated using the eq. 9 [43].

$$I = \frac{\sqrt{K(z)}}{\bar{u}(z)} \tag{9}$$

wehre $K(z)$ is turbulent kinetic energy and $\bar{u}(z)$ is mean velocity profile. Resultant mean velocity and turbulent

intensity profile at inlet, middle and exit of the computational domain are given in Fig.6. Note that turbulent intensity at the height of building is slightly less than 16% as provided by [7], however this difference is ignored for the current study.

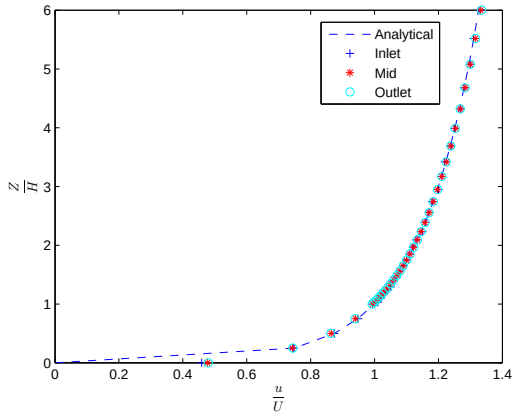

(a) Velocity profile

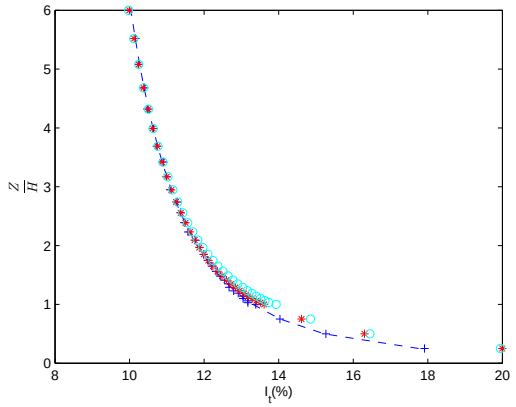

(b) Turbulence profile

Figure 6: Validation of boundary conditions for horizontal homogeneous ABL.

B. Turbulence Model Selection

We use two modified $k-\epsilon$ models namely, RNG-$k-\epsilon$ and $k-\epsilon$ EARSM, and one shear stress model (SST) and results are compared with field data [34], recent wind tunnel study [44] and LES performed by [45]. Unsteady RANS simulations as described in section II-A are performed in all cases and results are averaged after initial 20 timesteps. The mean pressure coefficient C_P is calculated by employing eq. 10 at the centre line of TTU building.

$$C_P = \frac{2(P - P_{ref})}{\rho {U_{ref}}^2} \tag{10}$$

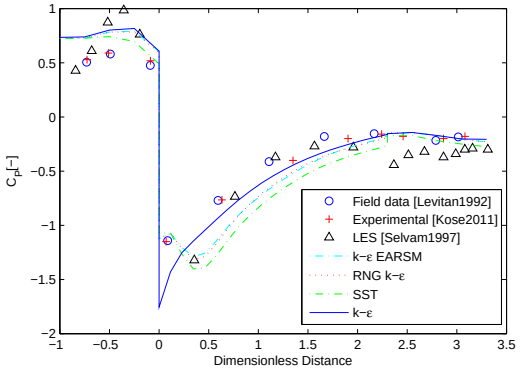

Figure 7: Mean pressure coefficient at the centre line of TTU building (parallel to 9.1m wall) with different RANS turbulent models

Pressure coefficient is over estimated on the windward face by all the turbulence models as shown in Fig.7 where SST model predicts better than the other two. RNG $k-\epsilon$ and $k-\epsilon$ EARSM predict the roof top pressure coefficient better than standard $k-\epsilon$ and SST turbulence with standard $k-\epsilon$ performing the worst as already explained in [35, 45, 46]. On leeward face SST performs best and predicts the pressure coefficient fairly accurately compared with wind tunnel and field data. The rest of the models behave same on the leeward wall i.e. slightly over predicting the pressure coefficients. Overall SST models perform better on windward and leeward wall with slight over estimation on the roof top compared to the rest three turbulence models. Whereas RNG $k-\epsilon$ and $k-\epsilon$ EARSM almost behave similar and are better on the roof top. It is to be noted that computational results of [45] using LES are very close to field data on the roof top whereas there is over estimation of pressure coefficient on windward and leeward walls. Results reported by [47, 48] using $k-\epsilon$ models do not show much deviation on windward face. Refs. [47, 48] did not use consistent boundary conditions as proposed by [3], however [35] did and reported similar over estimation on the windward face by all turbulent models. Another distinguishing fact is that their computations were done using steady state RANS compared to current study where unsteady formulation is used and results are averaged after all the time steps to obtain the mean pressure coefficients. Therefore a steady state solution is also considered using RNG $k-\epsilon$ turbulence model

(SS RNG $k-\epsilon$) and results are shown in Fig.8 along with the previous results. Steady state solutions with others are also done but not included as they do not show any improvement. It can be seen that steady state solution predicts the wind loading on the windward side superior than unsteady cases. Also it does not show small pressure reduction on roof corner as exhibited by all current unsteady computational studies as well as LES by [45].

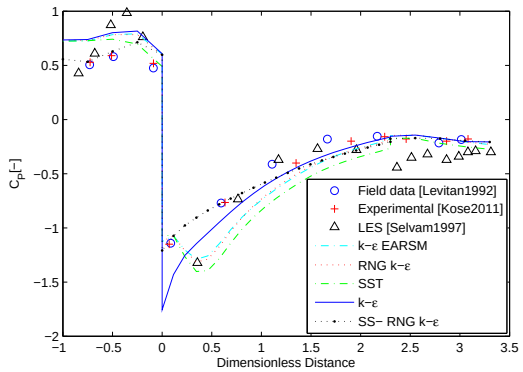

Figure 8: Mean pressure coefficient at the centre line of TTU building (parallel to 9.1m wall) with steady and unsteady RANS

Mean horizontal velocity ($\frac{u}{U_{ref}}$) contours are shown in Fig. 9 where standard $k-\epsilon$ and RNG $k-\epsilon$ don't capture the roof top vortex, although RNG $k-\epsilon$ shows a small circulation field. Whereas SST model resolves windward roof corner vortex successfully. To resolve such turbulent scales with $k-\epsilon$ models will require a dense mesh because over prediction of turbulent energy and hence eddy viscosity encourages the mixing of turbulent scales near the corner and flow separation does not occur distinctly. Similar conclusions were presented by [35]. All variants of eddy viscosity turbulence models used in the current study except standard $k-\epsilon$, predict the wind loading fairly good on low rise building and therefore can be potential candidates for further investigation in our application. From a designer point of view, since SST is slightly over predicting with the right trend, therefore it offers a conservative design. Furthermore it can capture corner vortices (if any) present in the flow at much less computational cost than other eddy viscosity models, thus we plan to use SST model in further study.

IV. Results and Discussion

Steady state RANS simulation is performed using SST turbulence model for all the cases unless otherwise mentioned specifically. Monitor points near the sunshade are placed to observe velocity, pressure, turbulent kinetic energy and eddy dissipation rate during iterative solutions. A stringent convergence criteria where all r.m.s. residuals are below 1×10^{-8} is set for solution stoppage. Convergence is also considered to be achieved if there is no evident change in variables at the monitor points and all r.m.s. residuals are below at least 1×10^{-6} as outlined in [49]. An example is shown in Fig.10 where it can be seen that all results at monitor points defined on the top and below surface of sunshade have achieved steady state solution. A zero degree (flow parallel to chord length of sunshade) of wind incidence angle (α) is simulated in all the cases except the angle of attack study where it is varied to find out the extreme loading scenario.

Table IV: Mesh convergence study for sunshade

Mesh	Elements	Nodes	Size
CaseA	891964	227412	$(27\times34\times59)$
CaseB	2025322	423093	$(35\times43\times74)$
CaseC	2473213	499689	$(43\times52\times92)$

CFX is a $3D$ solver and therefore sunshade should be given a thickness in order to satisfy the run requirements. A non dimensional thickness ($\frac{th}{L}$) of 0.002 is selected after a comparative analysis (not presented here). Three sets of mesh namely CaseA, CaseB and CaseC are generated where number of elements are increased in each case for studying mesh convergence study. Geometric progression of 1.1 is used in all cases which is less than maximum of 1.3 recommended by [25]. Details of mesh cases is shown in Table IV. Increase in number of elements in CaseB and CaseC is 2.27 and 2.77 times compared to CaseA which is less than recommended value of 3.4 recommended by COST [24]. Note that in current study ANSYS Academic version is used which has limitation of 512 thousand nodes and satisfying requirement of COST would require more nodes than allowed by program, therefore a relatively small fine to coarse ratio is used.

Results on the upper and lower surface at the centre line of sunshade for all three cases are shown in Fig.11. Mean pressure coefficient (C_P) on the lower surface is same for CaseB and CaseC setups while suction on windward side of sunshade is overestimated in CaseA. However on the upper surface except for the windward corner where CaseC shows the most suction, results from all three cases are practically identical. As explained earlier, a finer mesh than this is not possible using the academic version of CFX, therefore Case B where results do not vary significantly from CaseC, as a compromise

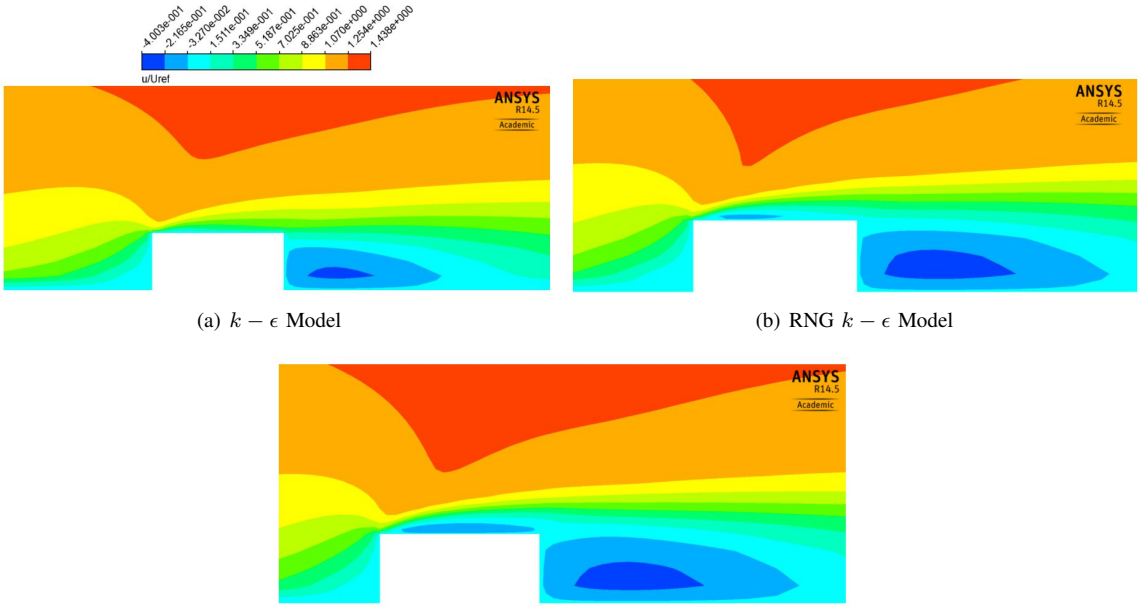

(a) $k-\epsilon$ Model

(b) RNG $k-\epsilon$ Model

(c) SST Model

Figure 9: Dimensionless velocity contours at the center plane of TTU building.

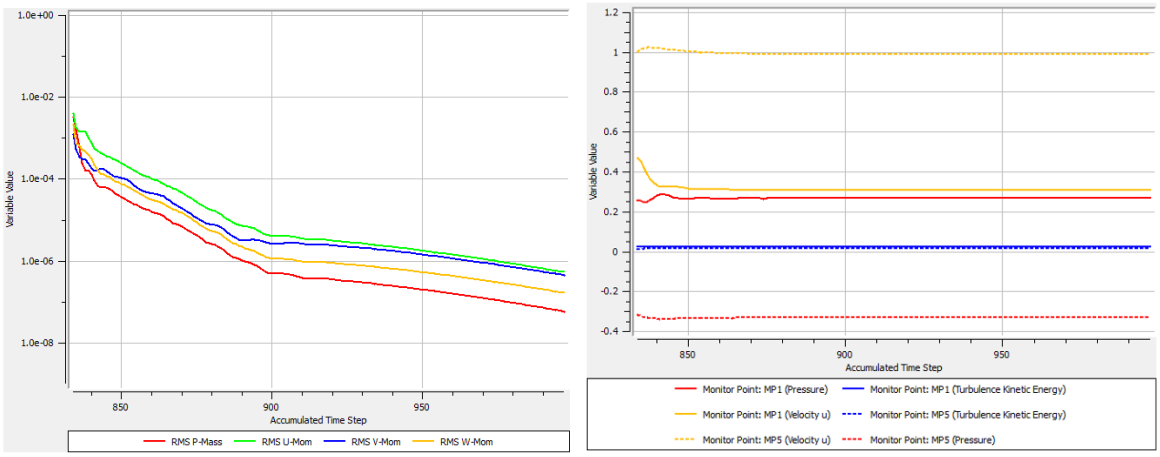

(a) R.m.s residuals

(b) Monitor points

Figure 10: An example for solution convergence history

on computational time and accuracy CaseB is chosen for next sections.

$$C_N = C_{P,U} - C_{P,L} \tag{11}$$

To investigate the effect of wind incidence angle or angle of attack (α) on pressure loading over sunshade, angle of attack is varied from 0^o to 240^o with increment of 30^o. In each case all the mesh is kept constant as the CaseB discussed earlier and central block meshed with unstructured tetrahedrons is rotated according to incidence angle. Such an unstructured mesh discritization allowed to change the angle of attack without changing the mesh of whole computational domain saving considerable amounts of time required for remeshing. Steady state cases with solver settings as discussed earlier are used for this study as well. However due to fast solution

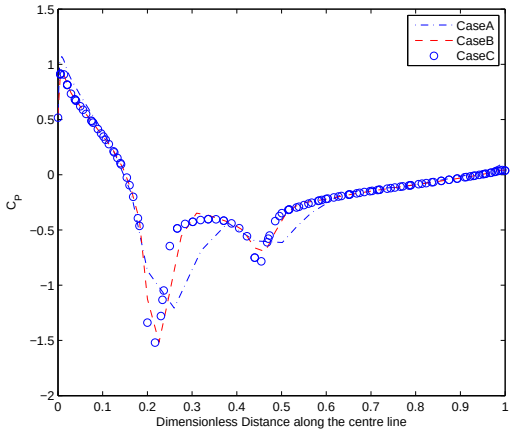

(a) Upper surface

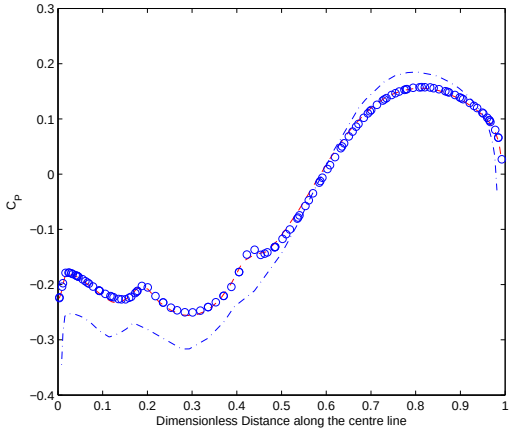

(b) Lower surface

Figure 11: Comparison of mean C_P for different mesh setups.

and easy convergence offered by standard $k-\epsilon$ model, it is used in this investigation. It has been established from validation study and by [23–25, 49, 50] that standard $k-\epsilon$ model over estimates the pressure coefficients on the windward side but it essentially behaves in the same way as other eddy viscosity models. Therefore in order to have an idea for the worst case scenario, it can be utilized without any problem in present section. Finalized loading to be used for structural analysis will therefore be found out using a case with worst case scenario and SST turbulence model separately. As the mesh points over the surface of sunshade are not same in case of different angle of attack scenarios, therefore in order to compare the results, it is assumed that all data points on the center line are equidistant. This allowed an easy comparison of net mean pressure coefficient (C_N) for various cases along with real distribution on the upper and lower surfaces. Please note that this does not result in actual variation of mean pressure coefficient over center line length (equidistant assumption) rather it makes comparison easy to investigate the extreme loading scenario.

Results of the comparative study in the form of mean pressure coefficient C_P on upper and lower surfaces along with the net mean pressure coefficient C_N are shown in Fig.12. Net mean pressure coefficient is calculated using eq. 11. The worst loading scenario is simulated with a wind incidence angle (α) of 30^o where windward edge of sunshade experiences positive upwards pressure forces and leeward is under negative pressure loads. These results are in agreement with [14, 15] where maximum loadings are experienced at 30^o angle of attack for a free standing canopy roof. This is then followed by 0^o angle of attack which is also significantly higher than the rest of the cases, however lower than 30^o angle of attack. As before, windward face is under upward pressure loading and leeward side including top is experiencing suction. Results show that leeward side of sunshade is under net upwards loading in case of 130^o, 150^o, 180^o and 210^o where magnitude of these loadings is not significant as well, however it again shows negative pressure (suction) near trailing edge. From the results presented it can be concluded that a sunshade designed to withstand loading of 30^o wind incidence angle will survive the wind loadings caused by other wind directions.

In order to get the pressure caused from wind loading, we perform a steady state analysis of full scale model at 0^owind incidence angle and compare the results with non dimensional case dealt earlier. After validation of 0^o case, wind direction of 30^o causing worst loading scenario as seen in previous section is also simulated on full scale to extract pressure loading for subsequent structural analysis. SST turbulence model is used for both cases in order to be consistent with previously investigated scenarios. Geometry and domain are modeled at $1:1$ scale with sunshade thickness of $5mm$ corresponding to non dimensional thickness of 0.002 analyzed earlier. Values of boundary conditions are altered, however profiles still remain the same given by eq.3 to 6. Surface roughness of the terrain (z_o) is given the value of $17mm$ as provided by [22]. All these boundary conditions resulted in a homogeneous ABL profile validated in an empty computational domain as shown in Fig.13.

Comparison of non dimensional and full scale models

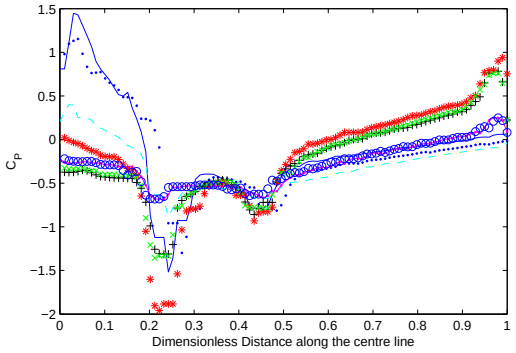

(a) Upper surface

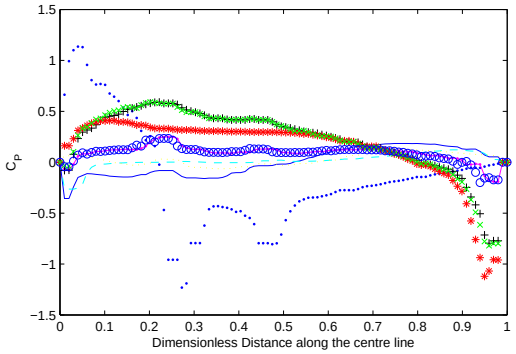

(b) Lower surface

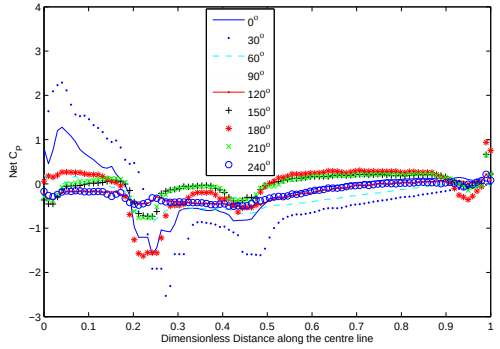

(c) Mean net pressure coefficient C_N for various angle of attacks.

Figure 12: Mean pressure coefficient C_P for various angle of attacks.

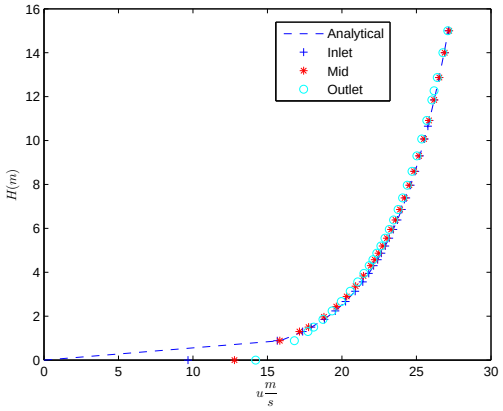

(a) Velocity profile

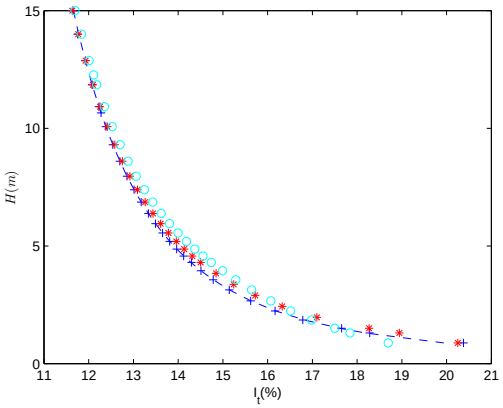

(b) Turbulence profile

Figure 13: Validation of boundary conditions for horizontal homogeneous ABL in case of 1:1 model.

for 0^o wind incidence is shown in Fig.14 where a reasonable agreement between the two can be seen. Small discrepancies can be associated with discritization errors and model constants difference between two scales. For our analysis purposes, we ignore these differences.

Results for pressure contours on upper and lower surfaces of sunshade in both wind directions are shown in Fig.16. It can be understood that flow is impinging on the windward side causing maximum pressures of 253.9Pa and 260.682Pa for 0^o and 30^o wind directions respectively. On a general overview it is seen that pressures on the upper surface are extreme in case of 30^o wind incidence angle where maximum suction of -718Pa is observed compared to -573Pa in case of 0^o case. Similar is the case with lower surface where maximum suction pressure of -356.6Pa occurs in case of 30^o compared to -203.76Pa in 0^o wind direction. Pressure loading symmetry is observed in case of parallel flow as shown in Fig.16(a) which was anticipated. In case of 30^o wind direction, corners parallel to incoming flow are under less suction forces compared to the others where extreme suctions are observed for the case (Fig.16(c)). Overall loadings on both upper and lower

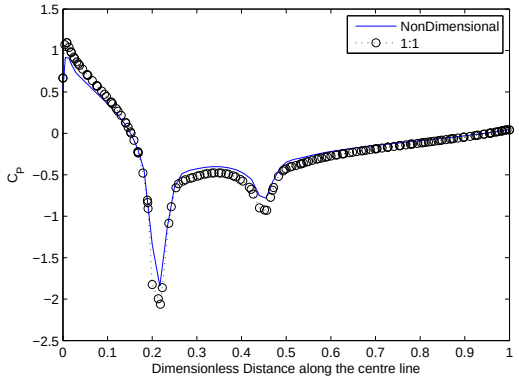

(a) Upper surface

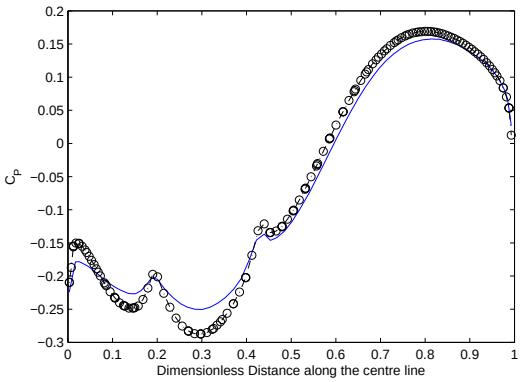

(b) Lower surface

Figure 14: Wind loading comparison between non dimensionalized and 1:1 models.

surfaces are higher in 30^o case that has already been discussed earlier.

A simple approach to extract wind loading from $1:1$ computational studies of 0^o and 30^o is used where we find area weighted averaged pressures P_{av} on upper and lower surfaces of sunshade using eq.12. Here P_i, A_i denote elemental pressure and area on a given surface respectively, N is the total number of elements and A_k is the total area of the respective subregion. Upper and lower surfaces are divided into five sub regions as shown in Fig.15. Area weighted average is used as advised in ANSYS help [26] because average of nodal values will be biased towards regions of higher mesh density. A Similar strategy has been mentioned in Chinese Building code as utilized by [51] for conducting structural analysis of heliostat mounting structure using ABL wind tunnel results.

$$P_{av,k} = \frac{\sum_{i=1}^{N} P_i A_i}{A_k} \tag{12}$$

Table V: Pressure (Pa) of sub-regions for 0^o wind incidence angle

Sub region	Upper Surface	Lower Surface	Net
1	70.96	-62.06	133.03
2	-77.01	-26.39	-50.61
3	-59.09	27.28	-86.37
4	-77.49	-30.45	-47.05
5	-170.39	-57.27	-113.13

Table VI: Pressure (Pa) of sub-regions for 30^o wind incidence angle

Sub region	Upper Surface	Lower Surface	Net
1	43.86	-65.26	109.12
2	-32.03	-38.47	6.44
3	-79.62	53.57	-133.188
4	-90.74	-2.40	-93.14
5	-181.63	-34.62	-147.02

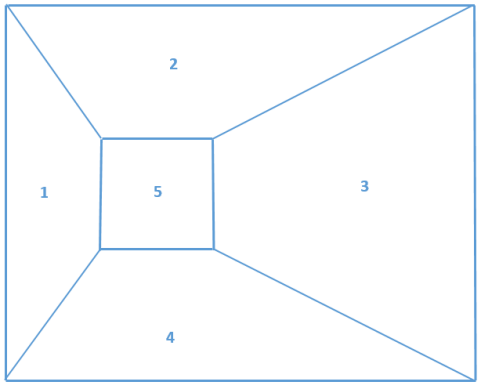

Figure 15: Division of upper and lower surfaces into sub regions for average pressure extraction.

Wind incidence angles of 0^o and 30^o realized worst loading scenario as seen in previous section, therefore we present pressures from both cases to be applied on structure. Subregion 1 is under net positive pressure in both cases with maximum loading of 133.03Pa in 0^o angle of attack. Subregions 3, 4 and 5 are experiencing suction forces with maximas in 30^o case. However subregion 2 is under higher suction of -50.61Pa in 0^o case as compared to net upwards pressure of 6.44Pa in 30^o wind direction. In order to design sunshade, we use extreme net pressure values from both cases for performing structural analysis.

Pressure loads are applied on respective areas (Fig.15) as per TableV and TableVI. Worst loading scenario for each patch is selected from 0^o and 30^o wind incidence angle cases. It has been assumed that connection of solar panel on the top and sunshade cap will be done

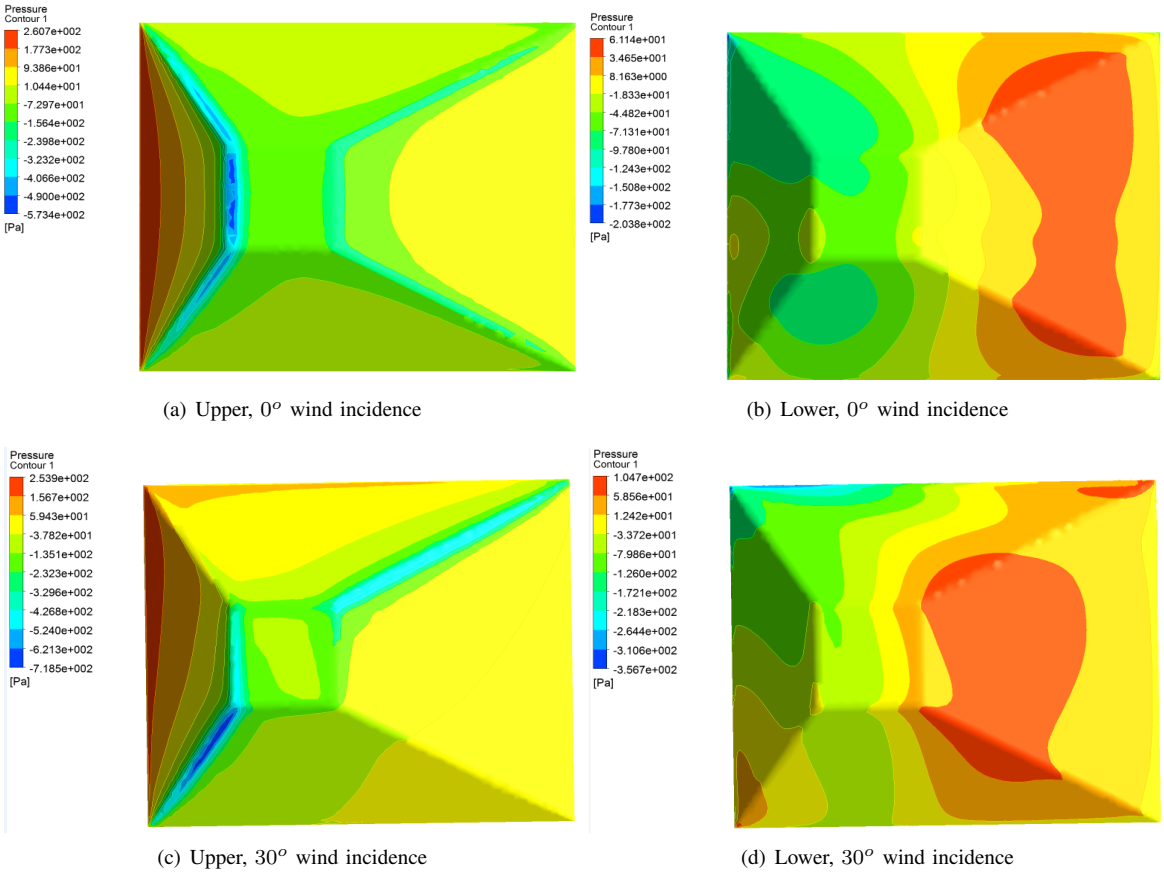

(a) Upper, 0^o wind incidence

(b) Lower, 0^o wind incidence

(c) Upper, 30^o wind incidence

(d) Lower, 30^o wind incidence

Figure 16: Pressure on the upper and lower surfaces of sunshade for two wind incidence angles.

using small bolts and therefore areas Area5 and Area6 in Fig.17(a) are constrained in all degrees of freedom i.e. no translational as well as rotational motion is allowed at these nodes.

To verify the mesh independence of results, three cases CaseA, CaseB and CaseC are studied. For comparison composite case is considered. Increase in the number of elements from CaseA to CaseB and from CaseB to CaseC is 4.53 and 2.84 respectively. Maximum deflection and stresses in first and last layer of sunshade are compared for all the cases as shown in TableVII. It can be seen that maximum deflection does not change much between cases and is $26.1mm$ in most refined case compared to $26.21mm$ in case of medium sized mesh (CaseB). Maximum stresses observed in first and last layer of composite sunshade cap show that the maximum property variation from CaseB to CaseC is 7.52% compared to 41.2% from CaseA to CaseB. Thus we use CaseB for any further results.

Sunshade top skin completely made of composite hand layup of 30 cloth layers is selected to present the results. Evolution of total deflection for top layer (30^{th}) at various load steps is presented in Fig.21 where it can be seen that rear tip of the canopy is showing deflection of $26.1mm$ which is quite significant for a structure with chord length of $2.5m$. Stresses developed on the other hand are not significant and are well below ultimate strength of composite laminates. Maximum stress encountered in x direction (σ_x) between first and last layer can be seen in Fig.18 which is only 4.43MPa where limiting strength of fiber glass fabric reinforced composite is 280MPa [29]. Similar behavior is observed in y direction where maximum stress (σ_y) is merely 6.27MPa in the first layer as shown in Fig.19.

One reason of such low stress levels is high value of deflection for the assembly. As stress signifies the internal resistance of the structure, due to high deflection composite material is not developing significant resistance against applied load. Another reason associated with a big deflection is the absence of any stiffeners (sup-

Table VII: Mesh independence results for composite design case

Result	CaseA	CaseB	Change (%)	CaseC	Change (%)
Max. Deflection (mm)	26.57	26.21	-1.35	26.10	-0.42
$\sigma_{x,max}$(MPa) First layer	3.5	3.71	6	3.75	1.07
$\sigma_{y,max}$(MPa) First layer	5.05	6.78	34.25	6.27	-7.52
$\sigma_{x,max}$(MPa) Last layer	4.12	4.37	6.06	4.43	1.37
$\sigma_{y,max}$(MPa) Last layer	1.81	2.57	41.9	2.4	-4.28
No. of Elemnts	1125	5100	353.35	14500	184.32

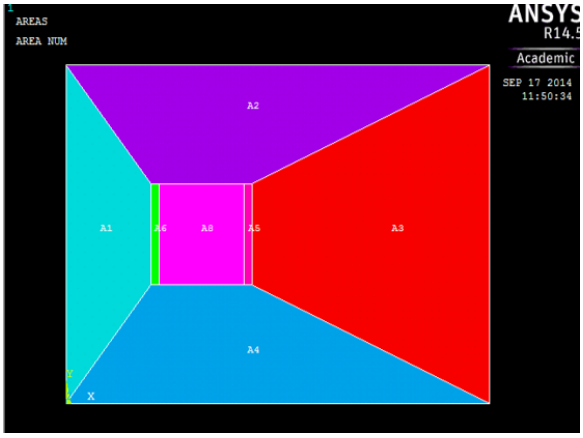

(a) Modeled geometry and area distribution

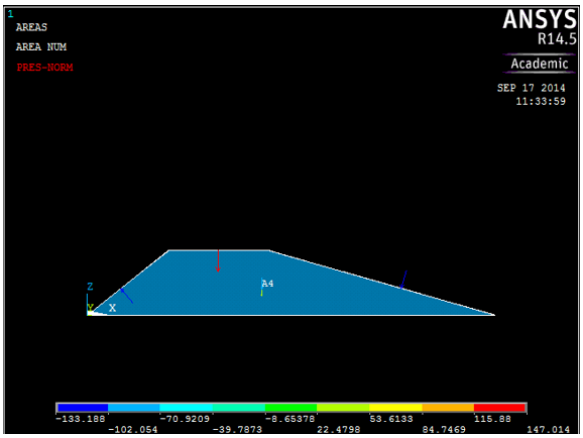

(b) Pressure load application

Figure 17: Geometry and boundary conditions

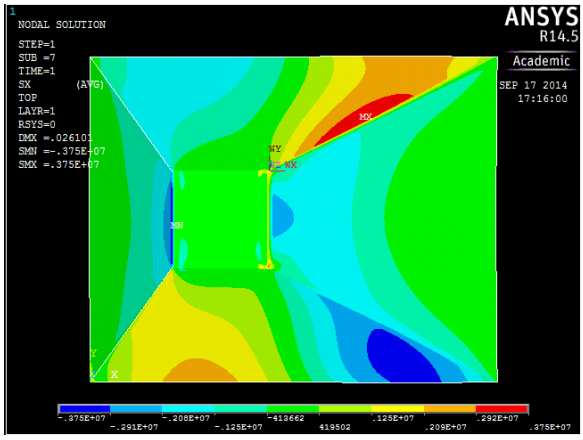

(a) First layer

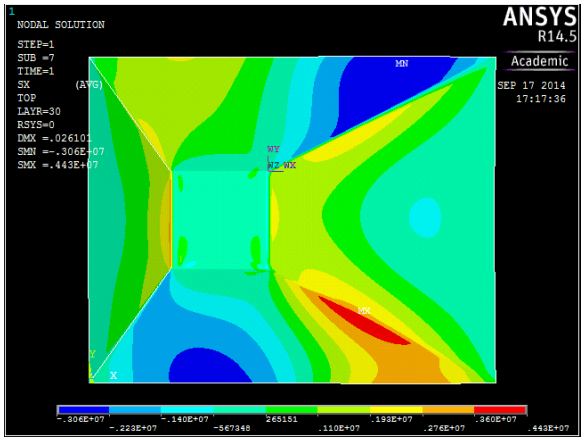

(b) Last layer

Figure 18: σ_x(MPa) in composite skin.

porting structure) underneath the composite assembly to hold it. Having metallic inserts during layup process of structural component comes with additional expense, therefore we do not explore scenario of having metallic stiffeners for maintaing shape of sunshade under wind loads.

However the scenario where all the structure is considered to be manufactured using standard industrial aluminum profile rods, deflection at the rear end of the sunshade cap is significantly reduced to $2.4mm$ compared to $26mm$ in case of composite material. Whereas von Mises stress used to gauge failure of metallic components comes out to be 10.4MPa which

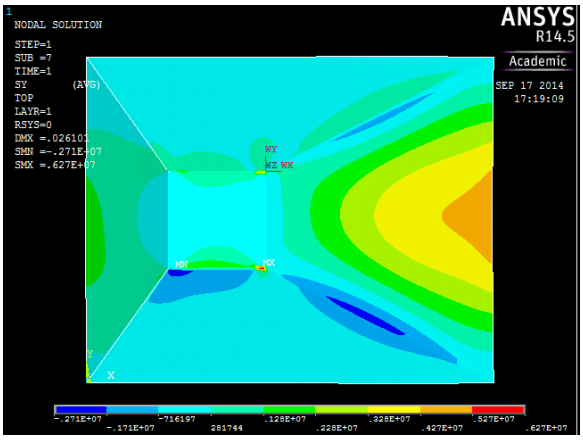

(a) First layer

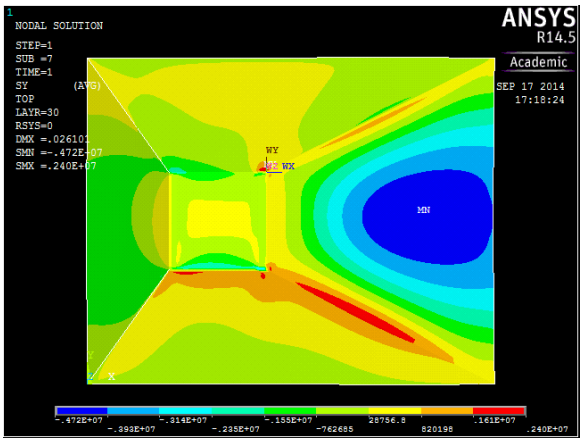

(b) Last layer

Figure 19: σ_y(MPa) in composite skin.

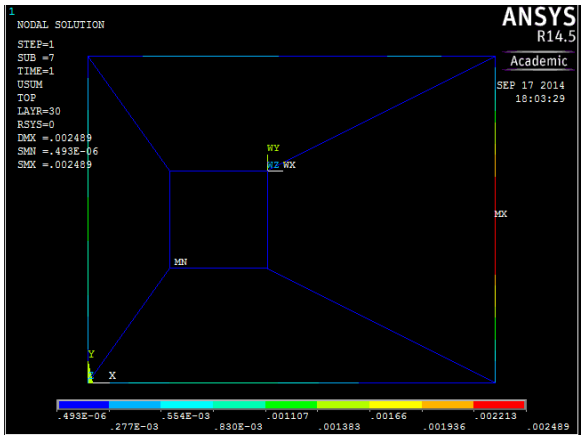

(a) Deflection (m)

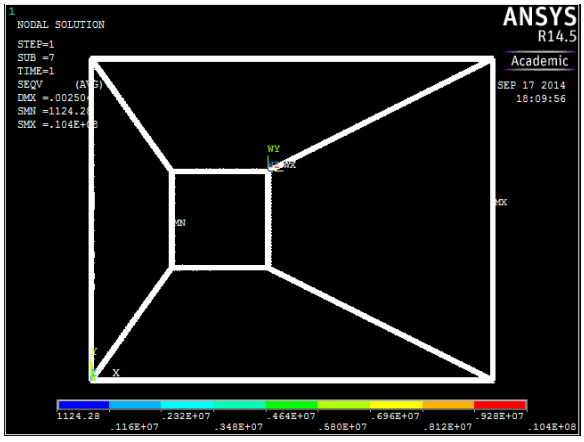

(b) von Mises stress

Figure 20: Results from metallic design case.

is well below the yielding limit of aluminum 20MPa as shown in Fig.20. This scenario also provides a safety factor of 1.92.

Comparing weight of the two designs, composite design without stiffeners and 30 layers of fiber glass plain weave fabric results in total mass of 55.78kg calculated using density and volume of modeled layer elements. On the other hand standard profiles from Alumil [31] results in total weight of 9.075kg with much less deflection. Composite design is studied for lighter and resilient design of sunshade, however current study shows that weight and overall deflection is not feasible compared to conventional metallic design with aluminum which shows quite practical deflection and stress levels. Maximum deflection is always observed at the rear end of sunshade which points out that in order to reduce it further, sunshade design might have to be revised and new wind loading dependent on new profile should be calculated which will in turn help to analyze integrity of structure.

V. Conclusions and Future Work

We performed CFD on the potential design of solar sunshade to analyze the pressure forces associated with fluid structure interaction. Velocity corresponding to Beaurofot scale of 9 was selected to perform fluid flow analysis. A relatively high velocity is chosen to simulate the gust like environment in reality. Based on the chord length of the sunshade, we performed CFD analysis at $Re = 3 \times 10^6$. Turbulence is another parameter that dictates magnitude of wind forces by causing shear distribution of the boundary layer. Normal levels of turbulence observed for low rise structures are in order of $15 - 20\%$ and based upon the validation study and potential application terrain characteristics, we simulated 16% turbulence at the height of the sunshade. Turbulence

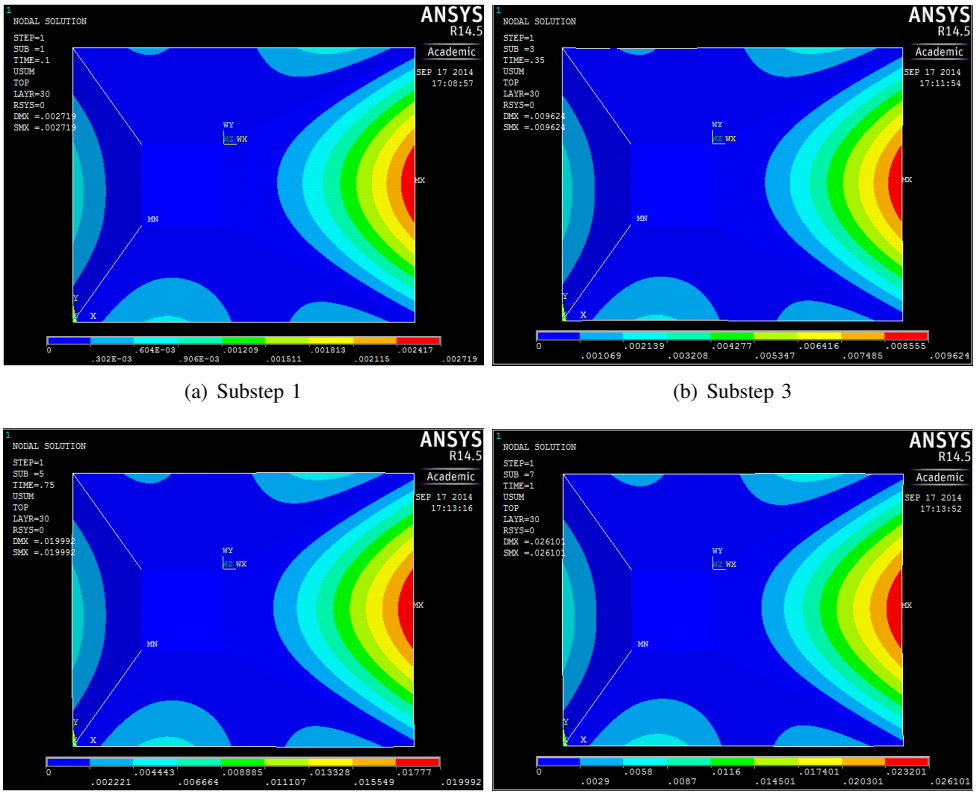

(a) Substep 1

(b) Substep 3

(c) Substep 5

(d) Substep 7

Figure 21: Deflection (m) observed during various load steps.

is modeled using SST eddy viscosity model or so to speak RANS formulation of Navier-Stokes equations. To estimate the worst loading scenario, 9 different wind directions are investigated with an aim to have qualitative understanding of force magnitude. To compare the results in between different wind incidence angle cases, net mean pressure coefficient (C_N) is calculated using mean pressure coefficients at the upper and lower skins of sunshade. Results show that extreme loading is expected at 30^o and 0^o wind flow directions. Windward side of sunshade experiences net positive upwards forces whereas leeward side is under suction forces. To cater for the dimensional effects, we then perform a $1:1$ scale CFD and to generate the pressure loading that can be readily used for subsequent structural analysis. After that we divide the sunshade in 5 zones where net mean pressure is calculated using area average pressure at each surface. This has led us to define a representative mean pressure to be applied on the individual surfaces for investigating structural response of the structure.

For carrying out the numerical analysis to estimate the structural integrity, we performed FEA where structure is divided into small elements and nodal solution of governing equations is found on the individual elements. Two alternative approaches for structural design are considered. Due to high specific strength and insulating properties of composites, fiber reinforced composite with E-glass plain weave fabric for the design of sunshade canopy is studied. Modeling was done using Shell181 element in ANSYS which allows to model lay up procedure as observed in industrial manufacturing of composites. Alternate study with aluminum pipes with hollow square cross section is also investigated where standard industrial aluminum profiles from Alumil [31] is used. Iterative methodology to reach upto reasonable solution is adopted where a programmable input file is written to be input in ANSYS that allows change in number of fabric layers in case of composite design and cross section of aluminum pipes in alternate design. It has been seen that without any internal structure (stiffeners), composite design with combined thickness of $5.4mm$ undergoes deflection of $26.10mm$ at the leeward end. Whereas design with aluminum pipes with a cross section of $20mm \times 20mm \times 2mm$ results in deflection

of only $2.4mm$ which is in practical range with von-Mises stress of 10.4MPa giving a design with safety factor of 1.92. Furthermore the resulting weight from aluminum design is 9.07kg compared to 55.78kg in the case of composite. Therefore a metallic design promises a lightweight and cheap solution for the sunshade under study and will be followed for manufacturing.

Although RANS is being used heavily in computational wind engineering, it still lacks the important scales of turbulence and hence LES should be pursued further to improve the design. Current work has been done using ANSYS Academic which is a student version of main commercial code and it has certain limitations. During the mesh refinement study of sunshade flow analysis, we could not achieve excellent grid independence due to program limitation of $512k$ nodes. This certainly has to be checked with full version for improved results. In present study wind loading has been characterized by mean pressure coefficients on the surface of sunshade, however in order to obtain peak pressure loadings transient study will be pursued in future that may lead to increased peak pressure loading.

Structural analysis performed misses engineering details of the final assembly. In order to improve results, top of the sunshade should be modeled along with bolts to see the effect of wind loading on the bolts and their yielding if any. Including these small details would not change the design substantially, however it will help deciding required dimensions and number of bolts necessary to hold the structure against incoming wind loads. Furthermore load is distributed using a thin metallic skin in case of aluminum design which does not represent the real case and is an approximation. Future work will be done to incorporate a pre-stressed cloth from manufacturers which however needs experimental testing to determine forces required to model pre-stressing of cloth using FEA.

REFERENCES

[1] E. Mathews, "Prediction of the wind-generated pressure distribution around building." *Journal of Wind Engineering and Industrial Aerodynamics 25, 219-228*, 1987.

[2] P. Richards and B. Younis, "Comments on "Prediction of the wind-generated pressure distribution around building" by E.H. Mathews." *Journal of Wind Engineering and Industrial Aerodynamics 34, 107-110*, 1990.

[3] P. Richards and R. Hoxey, "Appropriate boundary conditions for computational wind engineering models using k-ϵ turbulence model." *Journal of Wind Engineering and Industrial Aerodynamics 46-47, 145-153*, 1993.

[4] A. Aly, "Atmospheric boundary-layer simulation for the built environment: Past, present and future." *Building and Environment 75, 206-221*, 2014.

[5] C. Zhang, " Numerical prediction of turbulent recirculating flows with a $k-\epsilon$ model." *Journal of Wind Engineering and Industrial Aerodynamics 51, 177-201*, 1994.

[6] B. Blocken, T. Stathopoulos, and J. Carmeliet, "CFD simulation of the atmospheric boundary layer: wall function problems." *Atmospheric Environment 41(2), 238-252*, 2007.

[7] M. Levitan, K. Mehta, and W. Vann, "Field measurements of pressures on the Texas Tech building." *Journal of Wind Engineering and Industrial Aerodynamics 38, 227-234*, 1991.

[8] P. Richards and S. Norres, "Appropriate boundary conditions for computational wind engineering models revisited." *Journal of Wind Engineering and Industrial Aerodynamics 99, 257-266*, 2011.

[9] A. Aly and G. Bitsuamlak, "Aerodynamics of ground-mounted solar panels: Test model scale effects." *Journal of Wind Engineering and Industrial Aerodynamics 123, 250-260*, 2013.

[10] R. Pratt and G. Kopp, "Velocity measurements around low-profile, tilted, solar arrays mounted on large flat-roofs, for wall normal wind directions." *Journal of Wind Engineering and Industrial Aerodynamics 123, 226-238*, 2013.

[11] M. Shademan and H. Hangan, "Wind Loading on Solar Panels at Different Inclination Angles." in *Proceedings of 11th Americas Conference on Wind Engineering (CWE2010) San Juan, Puerto Rico*, 2009.

[12] A. S. of Civil Engineers, *Minimum design loads for buildings and other structures, Revision ASCE7-98*. American Society of Civil Engineers, Virginia

USA., 2013.

[13] G. Bitsuamlak, A. Dagnew, and J. Erwin, "Evaluation of wind loads on solar panel modules using CFD." in *Proceedings of Fifth International Symposium on Computational Wind Engineering (CWE2010) Chapel Hill, North Carolina, USA*, 2010.

[14] S. Gumley, "A Parametric Study of Extreme Pressures for the Static Design of Canopy Structures." *Journal of Wind Engineering and Industrial Aerodynamics 16, 43-56*, 1984.

[15] A. Poitevin, B. Natalini, and L. Godoy, "Pressures on open canopy structures with parapets under wind loading." *Engineering Structures 56, 850-867*, 2013.

[16] J. Diaz, P. Neito, and F. Dominguez, "Numerical analysis of pressure field on curved self-weighted metallic roofs due to the wind effect by the finite element method." *Journal of Computational and Applied Mathematics 192, 40-50*, 2006.

[17] J. Diaz, P. Neito, J. Perez, and A. Navarro, "Numerical analysis of the pressure field on curved and open self-weighted metallic roofs due to the wind effect by the finite volume method." *Journal of Applied Mathematics and Computation 209, 31-41*, 2009.

[18] D. Briassoulis and A. Mistriotis, "Integrated structural design methodology for agricultural protecting structures covered with nets." *Biosystems Engineering 105, 205-220*, 2010.

[19] A. Schellenberg, J. Maffei., K. Telleen, and R. Ward, "Structural analysis and application of wind loads to solar arrays." *Journal of Wind Engineering and Industrial Aerodynamics 123, 261-272*, 2013.

[20] A. Michelski, P. Kermel, E. Haug, R. Lohner, R. Wuchner, and K. Bletzinger, "Validation of computational fluid-struture interaction simulation at real scale tests of a flexible 29m umbrealla in natural wind flow." *Journal of Wind Engineering and Industrial Aerodynamics 99, 400-413*, 2011.

[21] A. Michalski, D. Britto, P. Gellene, and E. Haug, "Computational wind engineering of light weight structures." in *Proceedings of Sixth European and African conference on wind engineering*, Cambridge, UK, 2013.

[22] M. Levitan and K. Mehta, "Texas Tech field experiments for wind loads Part II: meteorological instrumentation and terrain parameters." *Journal of Wind Engineering and Industrial Aerodynamics 41-44, 1577-1588*, 1992.

[23] A. Tominaga, Y.and Mochida, R. Yoshie, H. Kataoka, T. Nozu, M. Yoshikawa, and T. Shirasawa, "AIJ guidelines for practical applications of CFD to pedestrian wind environment around buildings." *Journal of Wind Engineering and Industrial Aerodynamics 96, 1749-1761*, 2008.

[24] J. Franke, "Recommendations of the COST action C14 on the use of CFD in predicting pedestrian wind environment." in *Proceedings of 4th International Symposium on Computational Wind Engineering (CWE2006)*, Yokohama, Japan, 2006.

[25] J. Franke, A. Hellsten, H. Schlunzen, and B. Carissimo, "The Best Practise Guideline for the CFD simulation of flows in the urban environment : an outcome of COST 732." in *Proceedings of The Fifth International Symposium on Computational Wind Engineering (CWE2010)*, Chapel Hill, North Carolina, USA, 2010.

[26] ANSYSInc., "CFX Solver Theory Guide," 2014.

[27] A. Blicblau, M. Singh, E. McConnel, and M. Pleaner, "Stress analysis of a novice windsurfer sail by finite element analysis." *Journal of Mathematical and Computer Modeling 47, 1108-1116*, 2006.

[28] Y. Shindo, S. Takahashi, T. Takeda, F. Narita, and S. Watanabe, "Mixed-mode interlaminar fracture and damage characterization in woven fabric-reinforced glass/epoxy composite laminates at cryogenic temperatures using the finite element and improved test methods." *Engineering Fracture Mechanics 75, 5101-5112*, 2008.

[29] Y. Wang, J. Li, and D. Zhao, "Mechanical properties of fiber glass and kevlar woven fabric reinforced composites." *Composites Engineering 5(9), 1159-1175*, 1995.

[30] G. Belingardi, A. Beyene, and E. Koricho, "Geometrical optimization of bumper beam profile made of pultruded composite by numerical simulation." *Composite Structures 102, 217-225*, 2013.

[31] "AT & Standard Profiles 2014," availableathttp:// www.alumil.com/files/1/Products/, 2014.

[32] B. Blocken and C. Gualtieri, "Ten iterative steps for model development and evaluation applied to Computational Fluid Dynamics for Environmental Fluid Mechanics." *Environmental Modelling & Software 33 (2012), 1-22*, 2012.

[33] G. Richardson, A. Roberston, R. Hoxey, and D. Surry, "Full-scale and model investigations of pressures on an industrial/agricultural building." *Journal of Wind Engineering and Industrial Aero-*

dynamics 36, 1053-1062, 1991.

[34] H. Okada and Y. Ha, "Comparison of wind tunnel and full scale pressure measurement tests on the Texas Tech building." *Journal of Wind Engineering and Industrial Aerodynamics 41-44, 1601-1612*, 1992.

[35] T. Guha, R. Sharma, and P. Richards, "CFD modeling of wind induced mean and fluctuating external pressure coefficients on the Texas Tech University building," *Proceedings of 5th European African conference on wind engineering, Italy*, 2009.

[36] Y. Uematsu and N. Isyumov, "Wind pressures acting on low-rise buildings ." *Journal of Wind Engineering and Industrial Aerodynamics 82, 1-25*, 1999.

[37] M. Levitan and K. Mehta, "Texas Tech field experiments for wind loads Part I: building and pressure measuring system." *Journal of Wind Engineering and Industrial Aerodynamics 41-44, 1565-1576*, 1992.

[38] B. Launder and D. Spadling, "The numerical computation of turbulent flows." *Computer Methods in Applied Mechanics and Engineering 3(2), 269-289*, 1974.

[39] Y. Yang, M. Gu, S. Chen, and X. Jin, "New inflow boundary conditions for modeling the neutral equilibrium atmospheric boundary layer in computational wind engineering." *Journal of Wind Engineering and Industrial Aerodynamics 97(2), 88-95*, 2011.

[40] D. Hargreaves and N. Wright, "On the use of k-ϵ model in commercial CFD software to model the neutral atmospheric boundary layer." *Journal of Wind Engineering and Industrial Aerodynamics 95, 355-369*, 2007.

[41] A. Mochida, Y. Tominaga, S. Murakami, R. Yoshie, T. Ishihara, and R. Ooka, "Comparison of various $k-\epsilon$ models and DSM applied to flow around a high-rise building- Report on AIJ cooperative project for CFD prediction of wind environment." *Wind Struct. 5 (2-4), 227-244*, 2002.

[42] R. Yoshie, A. Mochida, Y. Tominaga, H. Kataoka, K. Harimoto, T. Nozu, and T. Shirasawa, "Cooperative project for CFD prediction of pedestrian wind environment in Architectural Institute of Japan." *Journal of Wind Engineering and Industrial Aerodynamics 95, 1551-1578*, 2005.

[43] J. Sullivan, R. Archer, and R. Flay, "Consistent boundary conditions for flows with in the atmospheric boundary layer." *Journal of Wind Engineering and Industrial Aerodynamics 99, 65-77*, 2011.

[44] D. Kose, D. Fauconnier, and E. Dick, "ILES of flow over low-rise buildings: Influence of inflow conditions on the quality of the mean pressure distribution prediction." *Journal of Wind Engineering and Industrial Aerodynamics 99, 1056-1068*, 2011.

[45] R. P. Selvam, "Computations of pressures on Texas Tech University building using large eddy simulation." *Journal of Wind Engineering and Industrial Aerodynamics 67 & 68(3), 647-657*, 1997.

[46] ——, "Computation of flow around Texas Tech building using $k-\epsilon$ and Kato-Launder $k-\epsilon$ turbulence model." *Engineering Structures 18(11), 856-860*, 1996.

[47] ——, "Computation of Pressures on Texas Tech Building." *Journal of Wind Engineering and Industrial Aerodynamics 41-44, 1619-1627*, 1992.

[48] A. Mochida, S. Murakami, M. Shoji, and Y. Ishida, "Numerical Simulation of Flowfield around Texas Tech Building by Large Eddy Simulation." *Journal of Wind Engineering and Industrial Aerodynamics 46 & 47, 455-460*, 1993.

[49] J. Franke, C. Hirsch, A. Jensen, H. Krus, M. Schatzmann, P. Westbury, S. Miles, J. Wissie, and N. Wright, "Recommendation on the use CFD in wind engineering," https://www.kuleuven.be/bwf/projects/annex41/protected/data/Recom

[50] T. Tamura, K. Nozawa, and K. Kodno, "AIJ guide for numerical prediction of wind loads on buildings." *Journal of Wind Engineering and Industrial Aerodynamics 96, 1974-1984*, 2008.

[51] C. Zang, B. Gong, and Z. Wang, "Experimental and theoretical study of wind loads and mechanical performance analysis of heliostats." *Solar Energy 105, 48-57*, 2014.